Atmospheric Measurements of HONO by Tunable Diode Laser Absorption Spectroscopy

C. L. SCHILLER [1], S. LOCQUIAO [1], TIMOTHY J. JOHNSON [2] and G.W. HARRIS [1]

[1] *Department of Chemistry and The Centre for Atmospheric Chemistry, York University, 4700 Keele St., Toronto, ON. M3J 1P3, Ontario, Canada, e-mail: corinnes@yorku.ca*
[2] *Battelle Pacific Northwest National Laboratory, PO Box 999, Richland, WA 99352, U.S.A.*

Abstract. Ambient gas phase nitrous acid (HONO) has been measured by Tunable Diode Laser Absorption Spectroscopy with sub-ppbv detection limits. An R-branch line in the 1263.4 cm^{-1} ν_3 band was found to be free of interference and suitable for ambient HONO measurements. Nitrous acid was measured during the night and early morning at an urban site in Toronto, Canada, during the summer of 1998. Average mixing ratios, integrated over 30 minutes, ranged from below the minimum detection limit of 300 pptv to 1.9 ppbv, with the highest concentrations observed during the early morning hours. During the night of 19 June 1998, the concentration of HONO increased by as much as 0.5 ppbv/hr. The usual decrease in HONO after sunrise was delayed by a few hours, possibly due to a combination of an increase in the production rate of HONO with rush hour, and attenuation of the early morning light by high NO_2 within the aerosol fog/haze.

Key words: atmospheric measurements, HONO, line strength, nitrous acid, tunable diode laser spectroscopy.

1. Introduction

Nitrous acid (HONO) plays an important role in the production of photochemical smog due to its accumulation at night (Platt *et al.*, 1980) followed by subsequent photolysis at sunrise. The photolysis of HONO is a direct source of hydroxyl radical:

$$HONO + h\nu(\lambda < 400\ nm) \rightarrow OH + NO.$$

The hydroxyl radicals thus liberated initiate and drive the oxidation of hydrocarbons in the atmosphere, as well as other species such as CO and SO_2. Nitrous acid thus directly affects the oxidative capacity of the atmosphere and indirectly contributes to secondary pollutants which are products of that oxidation.

Nitrous acid typically exhibits a strong diurnal variation with a nocturnal maximum and daytime minimum typically below current detection limits. Peak night-time concentrations have been measured in the range of 8.0 to 14 ppbv (Harris *et al.*, 1982; Appel *et al.*, 1990; Lammel *et al.*, 1996) for Los Angeles, while at a

rural site in the U.K., HONO mixing ratios as high as 2.0 ppbv have been recorded (Kitto and Harrison, 1992). Photolysis results in a rapid decrease in concentrations shortly after sunrise and HONO may thus play an important role as a source of OH when other photochemical activity is low (Harris *et al.*, 1982). This early morning pulse of OH may be characterised by measuring the decline of HONO during this time period, requiring a technique with not only good sensitivity but also with good temporal resolution.

Atmospheric sources of nitrous acid are, at present, not well characterised. Platt (1986) proposed three groups of possible source mechanisms: (1) Homogeneous gas-phase reactions, (2) Direct emission and (3) Heterogeneous production on surfaces of aerosols. Although homogeneous gas-phase production is likely to have little impact on the night-time production rate, direct emission and heterogeneous production on surfaces of aerosols are probably both important sources of the HONO accumulating during the night. Measurement of nighttime HONO with good spatial and temporal resolution should aid in understanding the production of HONO as well as possible loss mechanisms.

Although several laboratory studies of nitrous acid have been recorded (Saliba *et al.*, 2000; Kalberer *et al.*, 1999; Jenkins *et al.*, 1988; Pitts *et al.*, 1984; Sakamaki *et al.*, 1983; Akimoto *et al.*, 1987; Chan *et al.*, 1976), relatively few field measurements of HONO in the gas phase have been carried out. Atmospheric gas phase concentrations of nitrous acid were first measured using long path differential optical absorption spectroscopy (DOAS) in the near UV region (Perner and Platt, 1979) and have since been measure by a number of groups (Platt *et al.*, 1980; Harris *et al.*, 1982; Andrés-Hernández *et al.*, 1996; Febo *et al.*, 1996). This technique requires pathlengths generally greater than 1 km, and so the spatial distribution of HONO cannot be well resolved and DOAS is somewhat limited in that the species under study must have structured UV/Visible spectrum. Ambient nitrous acid has also been measured by collection on an alkali-coated Denuder, followed by analysis of NO_2^- by ion chromatography (Sjödin and Ferm, 1985; Allegrini *et al.*, 1987; Koutrakis *et al.*, 1988; Sjödin, 1988). The loss of NO_2^- due to oxidation to NO_3^- by O_3 (Sickles and Hodson, 1989) can lead to an underestimate of the HONO present, while the formation of HONO as an artifact on the Denuder (Sjödin and Ferm, 1985) can lead to an overestimate. A similar chemical method developed by Vecera and Dasgupta (1991) utilizes a diffusion scrubber coupled to an ion chromatography system to measure HONO. Since it is the nitrite ion that is measured, any gas phase species that yields NO_2^- in solution, (e.g., NO_2) acts as a potential interference. Recently Wingen and co-workers have developed a laboratory technique for measuring HONO that uses an excess of HCl to convert all the HONO to ClNO and measures the ClNO with FTIR spectroscopy (Wingen *et al.*, 2000).

Like FTIR and DOAS, the tunable diode laser absorption spectroscopy (TDLAS) method directly samples HONO in the gas phase, minimizing the possibility of the formation of artifacts, but at a higher sensitivity that FTIR due to the laser

source and with greater spatial resolution than DOAS due to point sampling. The method has been used successfully to measure a variety of trace species of atmospheric interest such as H_2O_2 and HCHO at sub-ppbv detection limits and averaging times of a few minutes (Fried *et al.*, 1997; Mackay *et al.*, 1996; Harris *et al.*, 1992; Harris *et al.*, 1989; Schiff *et al.*, 1983). This paper shows that TDLAS can be used as a sampling method for ambient HONO measurements with sub-ppbv sensitivity on ~30 minute time scales.

2. Experimental

2.1. HONO GENERATION AND CALIBRATION

TDL spectrometers normally require a 'reference' cell with sufficient concentration of the target molecule to provide an absorption signal that enables line locking for the diode laser. In addition to the line-locking function, the cell is required during the initial search for suitable lines free of atmospheric interferences.

The HONO reference cell used in these experiments employed the natural equilibrium between gas phase NO, NO_2 and H_2O (Stockwell and Calvert, 1978):

$$NO + NO_2 + H_2O \leftrightarrows 2\,HONO\,,$$

where $K_{eq}(atm^{-1}) = \exp(-15.56 + (4.73 \times 10^3/T))$. The HONO in the reference cell was found to be stable for long periods when using a mixture containing more H_2O and NO_2 than NO. A stable mixture of HONO was generated by combining 1 Torr of NO, 4 Torr NO_2 and 4 Torr H_2O. To minimize HONO and NO_2 photolysis the 10 cm long reference cell was kept covered at all times.

For calibration of the TDL spectrometer, gas phase HONO was generated by the reaction of gas phase HCl with solid $NaNO_2$ via the reaction:

$$HCl_{(g)} + NaNO_{2(s)} \rightarrow HONO_{(g)} + NaCl_{(s)}\,.$$

Gas phase HCl was produced by bubbling N_2 through a 0.5 M HCl solution. This HCl in the moist gas phase then reacted with solid $NaNO_2$ (>97% purity, Aldrich Chemical Company) to produce gas phase HONO. We note that if the HCl flow over the $NaNO_2$ is not kept moist, the HONO yield quickly reduces to low levels, presumably because the $NaNO_2$ surface becomes coated with NaCl. Vecera and Dasgupta (1991) observed similar results for HONO production from NH_4NO_2.

The concentration of HONO in the calibration flow was determined at the point of introduction of the flow to the ambient air inlet. The gas phase HONO was collected into two 15 ml samples of 1×10^{-5} M KOH solution in series, which were subsequently analysed for NO_2^- and NO_3^- using ion chromatography. Since NO_2 is also produced in the HONO generator and reacts in solution to form both NO_2^- and NO_3^- via;

$$2\,NO_{2(aq)} + H_2O \rightarrow NO^-_{2(aq)} + NO^-_{3(aq)} + 2\,H^+_{(aq)}$$

the NO_2^- measured and attributed to HONO must be corrected by the amount of NO_3^- present. Nitrous acid is slightly soluble in water ($H = 49$ M atm^{-1} (Seinfeld and Pandis, 1998). However, its solubility is enhanced by its dissociation into H^+ and NO_2^- in solution ($pK_a = 3.14$). In a basic solution (pH = 9), as was used here, however, the Henry's law coefficient for HONO is increased to 3.5×10^7 M atm^{-1}, due to dissociation, and HONO is collected with near 100% efficiency in the first collection tube in series. Moreover, NO_2 is only slightly soluble ($H = 1.0 \times 10^{-2}$ M atm^{-1} (Seinfeld and Pandis, 1998)), and comparable amounts should dissolve in both the first and second collection tube. Since NO is even less soluble than NO_2 ($H = 1.9 \times 10^{-3}$ M atm^{-1} (Seinfeld and Pandis, 1998)), any NO present would also be expected to dissolve in the second container as well as the first. Via the solution-phase reaction,

$$NO + NO_2 + H_2O \rightarrow 2\,NO_2^- + 2\,H^+ .$$

NO can lead to the production of nitrite but not nitrate, and since this reaction is nearly twice as fast as the self reaction of NO_2, this could lead to an error during calibration. However, the concentration of NO_2^- in the second sampler was nearly equal to the NO_3^- in that sample, indicating that there was little or no breakthrough of HONO and little, if any, NO present. The NO_3^- in the first container was ~1% of the NO_2^-, so even without a correction, NO_2 dissolution had little effect on the overall results.

The production of HONO from the reaction of gaseous HCl with solid $NaNO_2$ is a surface reaction, and therefore can change with time due to changing surface conditions, requiring frequent recalibrations of the HONO source. During the field measurements, the HONO calibration source samples were collected before and after each calibration of the TDLAS system, and each pair was subsequently analysed by ion chromatography.

2.2. FIELD STUDY SITE LOCATION AND INLET SYSTEM

The study was conducted in a mobile laboratory owned by Atmospheric Environment Services of Environment Canada, and located for the duration of this study at York University in Toronto, Canada. A 2 m tower on the roof of the mobile lab housed the Teflon inlet system, resulting in a total height above the ground of ~4.5 m. The mobile lab was located on one edge of a parking area and a large lawn. For calibration, the synthetic HONO gas was introduced as close as possible to the systems glass inlet orifice; the orifice reduces the pressure in the long path gas cell both for measurement and calibration. Upstream from the inlet aperture, the line was kept as short as possible to avoid the influence of the tower and inlet components. Thus, less than 0.5 m of inlet line was at atmospheric pressure before the inlet orifice, and the residence time within this section was ~0.5 seconds. Downstream from the inlet aperture, the line was at a reduced pressure of 30 Torr, resulting in a total residence time before the White cell of less than 1 second.

The inlet system did not contain a filter so aerosols were not excluded from the inlet. It is therefore possible that NO_2^- containing aerosols could interfere as the aerosols dry and out-gas HONO under low pressure conditions. Some of the ambient measurements reported here were made on relatively hazy/foggy early mornings, and so we now examine this potential interference further by considering the fraction of the HONO in the aqueous phase: At 298 K, the Henry's law coefficient for HONO is 49 M atm^{-1}. However, since the enthalpy of reaction is –9.5 kcal/mol (–40 kJ/mol) (Seinfeld and Pandis, 1998), the Henry's law coefficient increases to 85 M atm^{-1} at 288 K which was the average temperature during the measurements. Since HONO dissociates to form H^+ and NO_2^- in solution when the pH is above the pK_a (3.14 for HONO), increased dissociation would occur at higher pH's. The pH of clouds and fog can vary considerably from very acidic, e.g., pH $\approx$ 2 as measured near the southern California coast (Collett *et al.*, 1994), to neutral, pH $\approx$ 6.5 measured in a central California Valley. The pH of the haze was not measured during this study; however, using a conservative estimate of pH = 4.5 we obtain a modified Henry's Law coefficient for HONO of 1945 M atm^{-1}. The mole fraction of HONO in the aqueous phase is thus given by

$$\chi_{aq} = \frac{F_a}{1 + F_a} = \frac{10^{-6} \times H_{HONO} \times R \times T \times L}{1 + 10^{-6} \times H_{HONO} \times R \times T \times L},$$

where F_a is the fraction in the aqueous phase, R is the ideal gas constant 0.08205 atm L mol^{-1} K^{-1}, T is the temperature in Kelvin, L is the liquid water content of the fog or cloud in g m^{-3}, and H_{HONO} is the modified Henry's Law coefficient. Thus even at a relatively high liquid water content of 1 g m^{-3}, we would expect that only 4.5% of the HONO to be in the aqueous phase. As a consequence, even though a portion of the aerosols may be drawn into the cell, an overestimate of the gas phase HONO of at most 4.5% would be expected, which is acceptable.

2.3. INSTRUMENT SPECIFICATIONS

The broadband infrared spectra displayed in Figure 1 were recorded using a Bruker IFS 66v vacuum FTIR with 0.1 cm^{-1} resolution. For these measurements a Globar source, a Ge/KBr beam-splitter and a HgCdTe detector were used. The $NO/NO_2/H_2O$ mixture used to produce the HONO was held in a 13 cm cell with wedged and slanted windows.

The Tunable Diode Laser Spectrometer used for the field measurements was a modified T.A.M.S.-150 built by Unisearch Associates and on loan from the Atmospheric Environment Services of Environment Canada. The system uses wavelength modulation and 2f detection coupled with sweep integration for data acquisition. A complete description of the system can be found in Slemr *et al.* (1986).

A 1.5 m White cell with a folded pathlength of 126 m and total volume of 27 standard litres was used. A flow of 10 slm through the cell, at a reduced pres-

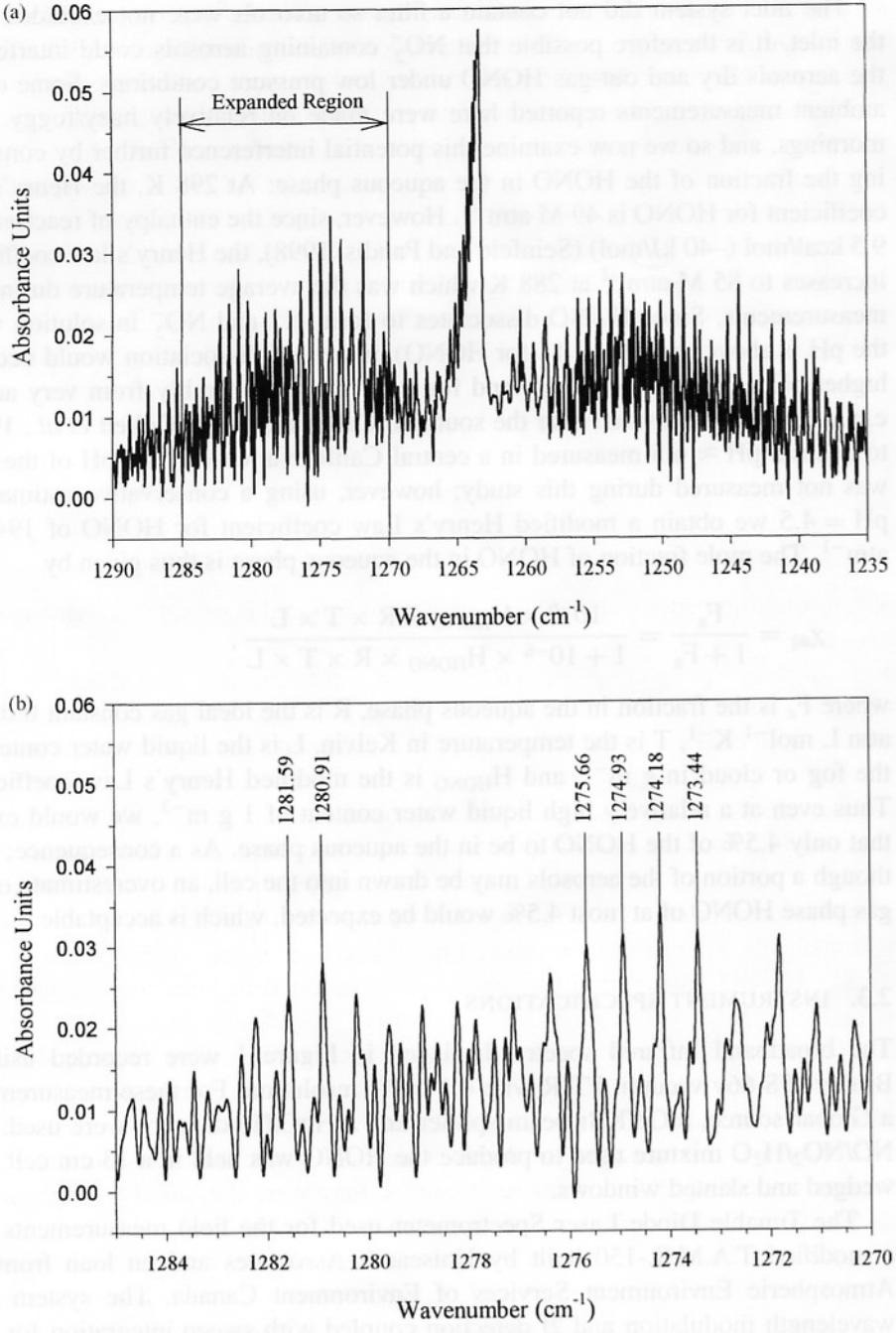

Figure 1. (a) 0.1 cm^{-1} Resolution FTIR Spectrum of the HONO band centred at 1263 cm^{-1}. (b) Enlargement of the 1270 to 1285 cm^{-1} HONO Spectrum.

sure of 30 torr, resulted in a residence time within the cell of ~6 seconds. To allow equilibration within the lines and cell, stabilization times of 1.5 minutes were used when switching between calibration, ambient and background modes, to help eliminate possible memory effects. Examination of an ambient spectrum following a calibration showed no residual calibration signature, indicating that 1.5 minutes was sufficient time to purge residual HONO from the system even following calibrations at fairly high concentrations. Ultra high purity air was used as both the carrier gas during calibration and as the background gas.

Spectra were recorded for one minute, in a cycle such that eight ambient measurements were taken for each background, and one calibration for each 6 backgrounds (i.e., every 48 ambient measurements). Including the stabilization times, this resulted in a calibration once every hour. Ambient and background spectra were subsequently averaged to 30 minute sampling intervals.

3. Results and Discussion

3.1. LINE SELECTION AND LINE STRENGTH DETERMINATION

The most prominent band of HONO in the mid-infrared is the trans-ν_3 band centred near 1263.4 cm^{-1} (Kagann and Maki, 1983). A 0.10 cm^{-1} resolution Fourier Transform infrared spectrum of this HONO band, between 1235 and 1290 cm^{-1} was obtained, and a reference spectrum of N_2O at the same resolution was subtracted from the HONO spectrum resulting in the spectrum shown in Figure 1(a). This spectrum for the ν_3 band of HONO is at a slightly higher resolution (cf. 0.5 cm^{-1}) and is consistent with the recent results of Barney *et al.* (2000) as well as those of Maki and co-workers (1988). TDL lasers originally acquired for studies of H_2O_2 near 1280 cm^{-1} were available and therefore suitable lines in the HONO R branch were examined more closely. Figure 1(b) shows an expanded view of the trans-ν_3 R-branch, showing several candidate lines that could be used with this laser.

The HONO lines within this band were examined to determine if they were strong enough to provide measurable optical densities for anticipated ambient concentrations. HONO line strengths measured by Becker *et al.* (1995) in the P-branch near 1255 cm^{-1} were 7 to 12×10^{-21} cm^{-1}/molecule-cm^{-2}, which when compared to measurements by Maki (1988) were found to differ by a factor of 2. Since our data show the line strengths in the R-branch are larger than those in the P, and there is some discrepancy in these strengths, they were measured by comparison to nearby N_2O lines which are listed in the HITRAN (1996) data base. A line strength of 3.25 ($\pm$0.17) $\times$ 10^{-20} cm^{-1}/molecule-cm^{-2} for the line centred at 1280.4 ($\pm$0.3) cm^{-1} was measured. This is comparable to the line strengths found for H_2O_2 (4.5×10^{-20} cm^{-1}/molecule-cm^{-2} (Brassington, 1994)) which resulted in TDL minimum detectable concentrations (MDC) of 50 pptv (1σ) for a 1 hour average using a similar TDL instrument (Schiff *et al.*, 1992; Mackay *et al.*, 1996). This suggests that the HONO line should be strong enough to allow measurement of HONO at concentrations well below 1 ppbv. A line near 1280 cm^{-1} was chosen

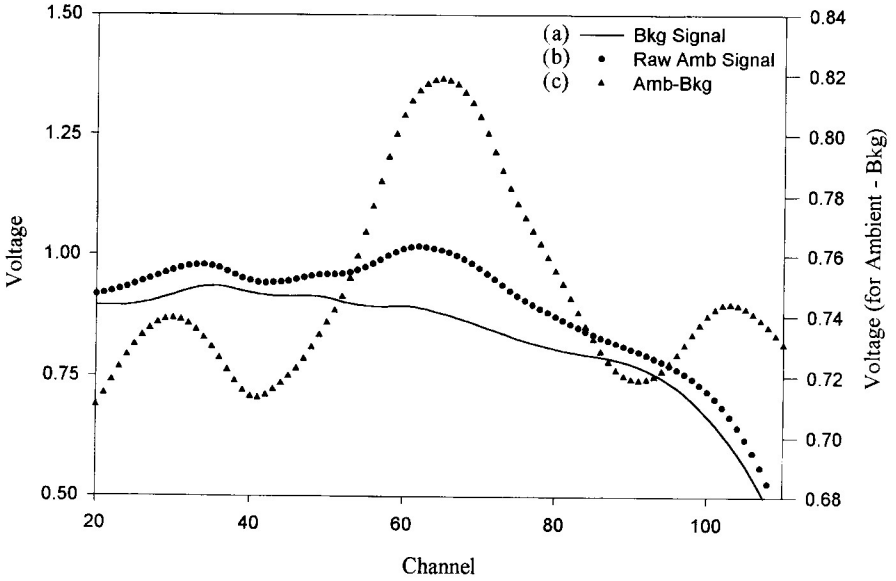

Figure 2. 30-minute averaged (a) background, (b) ambient and (c) ambient – background spectrum for HONO measured on 20 June, 1998 at 3:30 a.m.

thus for the ambient measurement phase. This line was found to be free of interference from water but lay on the wing of an adjacent weak N_2O line, which affected the symmetry of the observed signal.

Figure 2 shows the actual TDL ambient signal from this HONO line averaged for 30 minutes before and after background subtraction. Spectra are stored into 128 channels along the x-axis with 16 bit resolution on the y-axis. A definite HONO signal is apparent even before background subtraction. Subtraction of the background signal (curve b) resulted in a clean signal for ambient HONO (curve c). A comparison of the signal after background subtraction (Figure 3, curve a) with that of the 110 ppbv calibration spectrum for HONO (Figure 3, curve b) indicates an excellent reproduction of the shape of the spectrum for the 1.24 ± 0.18 ppbv ambient concentration measured.

A negative distortion in the signal shape in channels $>\sim 93$ can be seen in Figure 2 curves a and b, due to the wing of the N_2O absorption line located near our HONO line. Since both the background and ambient air contained N_2O, when the background is subtracted from the ambient, the absorption is minimized. However, examination of the right side of the result of background subtraction (curve 2c), showed a slight change in the symmetry of the resultant spectrum, indicating incomplete subtraction of the N_2O possibly due to the slight differences in N_2O concentration from ambient air and ultra high purity bottled air. We can examine the distortion separately considering the linear fit of the ambient and calibration spectra for channels <63 and >63. Figure 4 shows a plot of the background corrected ambient spectrum with that of the calibration minus background spectrum.

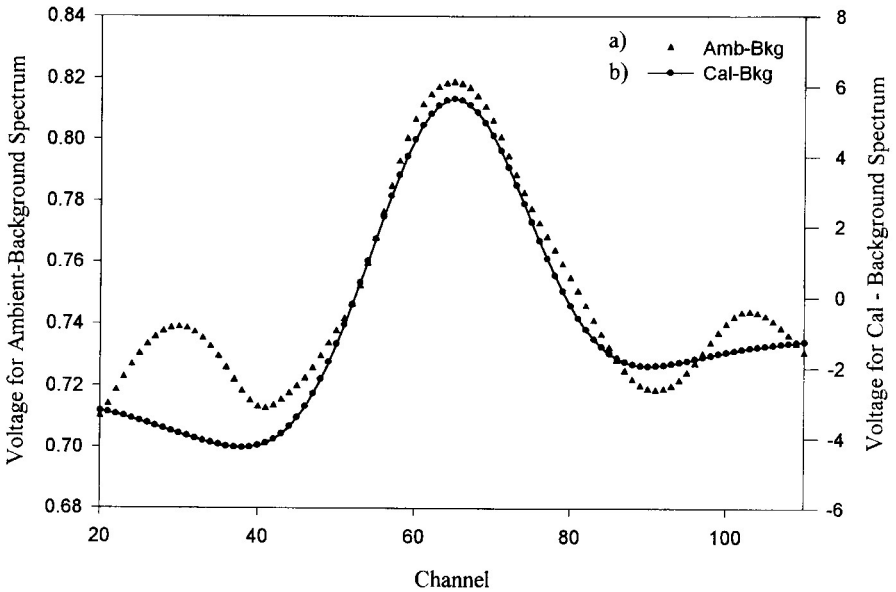

Figure 3. Comparison of the ambient minus background signal (a) compared to the calibration minus background signal (b) for HONO on 20 June 1998 at 3:30 a.m.

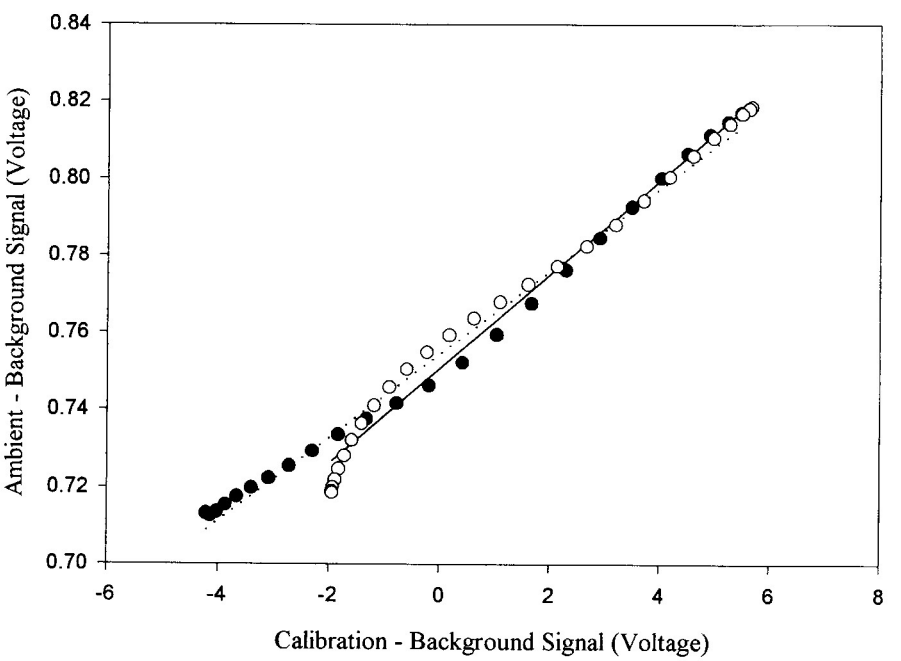

Figure 4. Linear fit of the ambient minus background HONO signal with the calibration minus background signal from 20 June 1998.

Channels below 63 are represented by the solid circles and its regression by the dotted line, while channels above 63 are represented by the open circles and the solid regression line. The regression parameters indicate a slope of 0.0108 and 0.0122 V/channel for the two methods of background subtraction, resulting in a 11% difference in the calculated HONO concentration. We can therefore surmise that by using the entire spectrum, an error of approximately 5.5% is introduced by the line shape distortion from the N_2O interference.

The minimum detectable concentration of HONO was determined by two successive one-minute background spectra of ultra zero air, where one was subtracted from the other. The resulting residual spectrum is then fitted to the calibration spectra and a concentration calculated. Since background spectra are subtracted from ambient spectra, by subtracting successive backgrounds and fitting the residual to the calibration, we can determine the noise level of the measurement. Using a number of these residuals we calculated the average minimum detectable concentration of HONO to be ~300 pptv (1σ). Signal averaging for 30 minutes should improve the minimum detection limit to better than 300 pptv.

The optical density at the minimum detectable concentration was estimated by assuming that the line used had a line strength of 3.25×10^{-20} cm^{-1}/molecule cm^{-2}, similar to that measured at 1280.4 cm^{-1}. At a detection limit of 300 ppt, the optical density was 4.7×10^{-5}. In previous studies, this instrument has measured HCHO with detection limits of 100 ppt or optical densities near 1.65×10^{-5}, suggesting that with a diode laser with better spatial mode quality, HONO detection limits of ~100 ppt may be achieved.

3.2. AMBIENT HONO MEASUREMENTS

HONO measurements were made on 4 consecutive nights in June of 1998. Temperatures remained relatively warm overnight (288–293 K), with relative humidity's remaining near 100%. Although the concentration of NO_2 was not measured during the campaign, a previous study at York University in 1994 showed the average NO_x concentrations in July range from 40 to 75 ppbv (Hastie, private communication). Measurements at various National Air Pollution Surveillance (NAPS) sites within Toronto showed NO_2 mixing ratios ranging from 25 to 60 ppbv on the nights measured, with concentrations building during the four days (NAPS, 1998, John Shelton, private communication). Wind speeds were light and variable during these four nights; such conditions appeared to favour the formation of HONO and its subsequent build-up during the course of the night.

Figure 5 shows the night and early morning HONO concentration from Thursday, 18 June through Sunday, 21 June, 1998. HONO concentrations ranged from below the detection limit of 300 pptv to ~1.9 ppbv, with HONO above detection limits for some time on each of the four nights. Figure 5(a) shows the 18 June HONO concentrations from 3 a.m. to 6:30 a.m. Concentrations rose to above ~1 ppbv in the early morning hours before falling abruptly to below the detectable

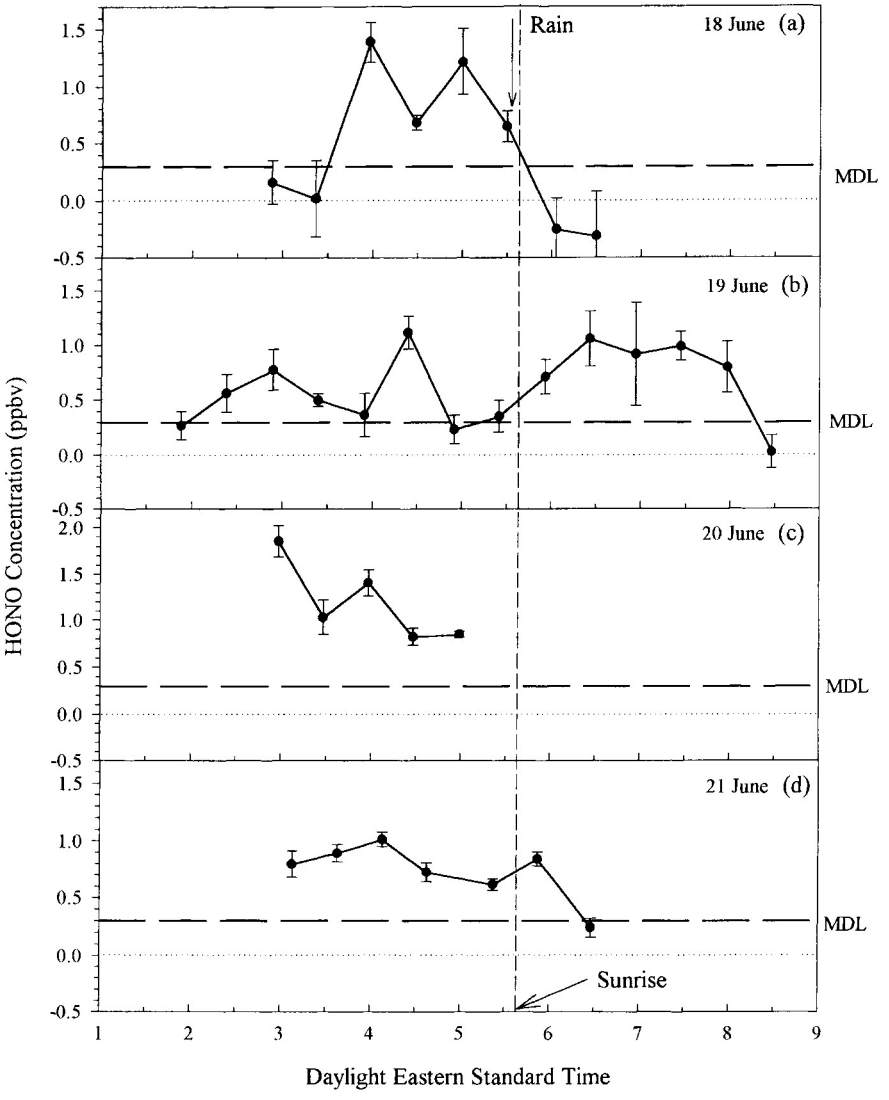

Figure 5. Ambient HONO concentrations measured on (a) 18, (b) 19, (c) 20, and (d) 21 June at York University in 1998. The error bars indicate 1σ standard deviation of the averaged spectra which may vary depending upon the fit of the individual background spectra.

concentration just before sunrise following a rain event. At 6:00 a.m., with a solar zenith angle of 86.3°, the photolysis rate of HONO under clear sky conditions is approximately 1.75×10^{-4} s^{-1} (Henderson *et al.*, 1987), resulting in a destruction rate of approximately 370 ppt/hr, which is consistent with the observed HONO loss. A similar early morning loss was observed on 21 June, Figure 5(d), with HONO concentrations decreasing from ~700 ppt to below the detection limit shortly after 6 a.m.

The highest HONO mixing ratios were observed during the night of 20 June (Figure 5(c)), coinciding with highest NO_2 concentrations, ~50–60 ppbv, observed at nearby NAPS sites (NAPS, 1998). Large changes in HONO concentrations over short times may indicate that a number of different air masses were sampled, emphasizing the need for good spatial and temporal resolution. Early morning rain, starting before 5 a.m., resulted in no data being available during this morning after sunrise.

19 June yielded the most complete data set which is shown in Figure 5(b). Concentrations began to rise shortly after midnight from below the detection limit to about 800 pptv at 3 a.m. The concentration then fell to near the detection limit indicating a possible change in airmass composition. Although the wind was light, it appears that a number of individual air masses were measured. This was apparent by the relatively large concentration of HONO observed for a short time at 4:30 a.m.

Near dawn, the HONO concentration reached a plateau of ~1 ppbv, which persisted well after sunrise, presumably indicating a balance between production and limited photolysis at the high zenith angle under hazy conditions. Between 8 a.m. and 8:30 a.m., the HONO was rapidly lost and concentrations fell to below the detection limit. With sunrise occurring at 5:36 a.m., HONO remained for ~2 to 2.5 hours longer than would be normally expected given its high photolysis rates. This may be explained by either an increase in the production rate of HONO, a decrease in its loss rate, or a combination of the two effects. We now further consider these two possibilities.

The loss of HONO by photolysis is fast under clear sky conditions, normally resulting in the concentrations of HONO decreasing rapidly shortly after sunrise. Delay of this decrease by attenuation of the incoming solar radiation would require >90% loss of the incoming radiation (Figure 6). The presence of early morning haze/fog may attenuate the incoming solar radiation, particularly at high solar zenith angles, however, water droplets are poor absorbers in the region of HONO photolysis. Due to the site location, which, depending on the wind direction, may be influenced by a freeway, it is possible that a fraction of the aerosol could be black carbon, which does absorb in the region of interest. However, black carbon would not be abundant enough to account for the attenuation required. Therefore, although absorption by aerosols may play a role in the delayed loss of HONO, it can not alone account for the delay.

Nitrogen dioxide (NO_2) is known to have a considerable absorption cross section within the region of HONO photolysis (Seinfeld and Pandis, 1998). Figure 7 shows the absorption cross section of HONO as well as the optical density that NO_2 would present to incoming solar radiation at varying solar zenith angles (SZA) calculated using a fixed NO_2 mixing ratio of 40 ppbv and a boundary layer height of 750 m. The optical density of NO_2, in the region above 350 nm where HONO photolysis is the greatest, can be >0.45 at a zenith angle of 85°, however this drops to below 0.10 at 65°. In addition, the effective pathlength within the boundary layer

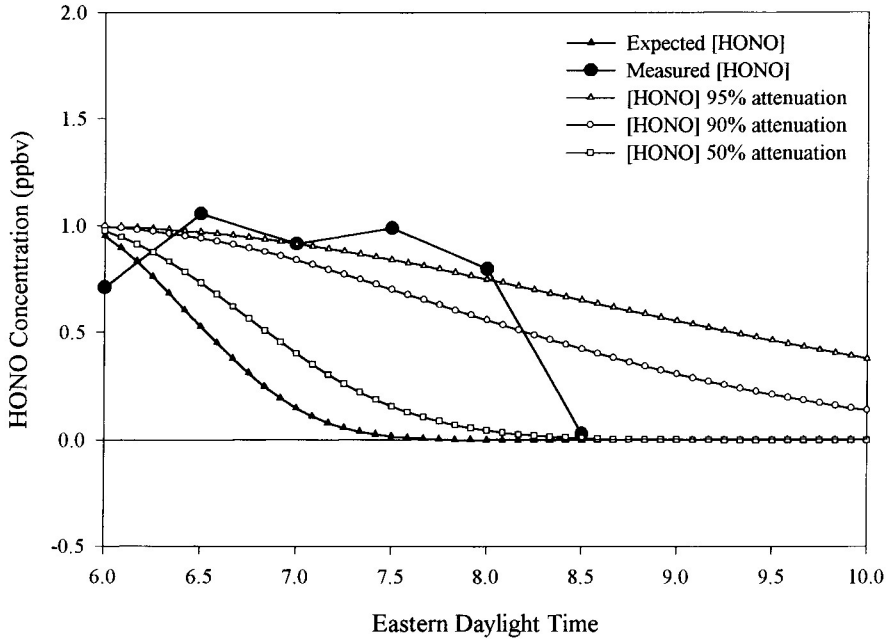

Figure 6. Decrease in the photolysis rate of HONO due to the attenuation of the solar radiation by 50%, 90% and 95%, compared to the measured HONO concentrations on 19 June between 6 and 8:30 a.m.

may be greater than the geometrically calculated one due to scattering within the haze thereby increasing the optical density of the NO_2. Thus it seems that attenuation of photochemical radiation through absorption by NO_2, or other species could noticeably delay the onset of rapid photolysis, but is unlikely to provide a full explanation for the 2–2.5 hour delay observed on 19 June. Therefore, in addition to abatement in the loss mechanisms, we consider other possible production mechanisms.

One additional source of HONO in the early morning could come from HONO in the aqueous phase diffusing into the gas phase, as the relative humidity falls after sunrise. However, as we stated earlier, the fraction of the HONO in the aqueous phase is likely to be less than 5%, and this would likely have little effect in delaying the decrease in HONO concentration at sunrise.

Ammann *et al.* (1998) have measured the production of HONO on fresh soot and found HONO production to be 1.0×10^{12} molecules s^{-1} per cm^2 aerosol surface at NO_2 concentrations of 12 ppbv. Using a black carbon aerosol loading (Berner *et al.*, 1996), of 10 μg^{-3}, a surface to volume ratio of 3×10^{-5} cm^{-1} and a yield of 3.3×10^{-4}, Ammann *et al.* (1998) calculated a conversion rate of NO_2 to HONO of 3.7×10^{-3} s^{-1} on fresh surfaces, and 1.1×10^{-4} s^{-1} on slightly aged surfaces. This rate was independent of the NO_2 concentration and relative humidity, but decreased with the aging of the carbon surface. At York University, with a freeway

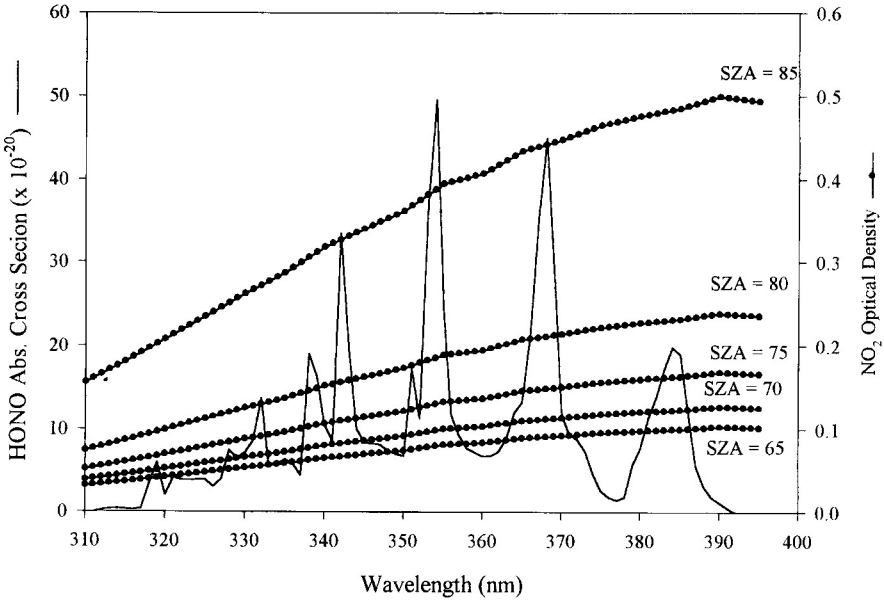

Figure 7. Wavelength dependence of the absorption cross section of HONO and the optical density of NO_2 as varying solar zenith angles (SZA) calculated from a fixed NO_2 mixing ratio of 40 ppbv and a boundary layer height of 750 m.

within 1 km and a number of busy streets much closer, diesel engines could supply fresh black carbon, which would impact the measurement site when winds are from the west. At 10 ppbv of NO_2, the production rates of HONO on black carbon aerosols could be >4 ppbv/hr. At York University at 7:30 a.m. on 19 June, the solar zenith angle is 71.5° resulting in a photolysis rate for HONO of $\sim 1.08 \times 10^{-3}$ s^{-1}. Therefore to maintain a HONO concentration of 1 ppbv, a production rate of 1.08×10^{-3} ppbv s^{-1} or 3.9 ppb/hr is required. Even with no attenuation of the incoming solar radiation, the production of HONO on black carbon could be high enough to balance this photolysis rate, and therefore could account for the HONO persisting well after sunrise on this day.

During the night of 19 June, HONO increased on two separate occasions (1:30–3:00 a.m.; 5:00–6:30 a.m.). The rate of increase was ~0.5 ppbv/hr during each period (0.50 ± 0.05 ppbv h^{-1} in the first and 0.55 ± 0.07 ppbv h^{-1} during the second). Harris *et al.* (1982) measured production rates of ~1 ppbv h^{-1} on 8 August 1980 at Riverside California, with a total NO_x concentration of 205 ppbv, and a maximum HONO concentration of 8 ppbv. Harrison and Kitto (1994) calculated that at NO_2 levels higher than 10 ppbv, the dependence of HONO production on NO_2, expressed as d/dt [HONO]/[NO_2], is 0.7–3.4% h^{-1}. HONO production rates of 0.5 ppbv h^{-1}, as measured in our experiment, could be produced with NO_2 concentrations as low as 15 ppbv, but likely require a concentration near 60 ppbv as extrapolated from Harrison and Kitto's (1994) best fit line. The large variation in

production rates may indicate that the formation is not only dependent on the NO_2 concentrations, but also on aerosol or black carbon loading as well. Since both NO_2 and black carbon are both produced primarily from combustion, their sources are similar, and high HONO production rates should correlate with peak traffic times.

Using the NO_2 concentration and an estimate of the black carbon content we can estimate the morning HONO production rate from that measured at night. The concentration of NO_2 during the morning rush hour was approximately 3 times higher than during the period of time when HONO production was monitored during the night (NAPS, 1998). In addition, since CO and black carbon have similar sources, CO may be used as an indicator of the amount of soot loading. Since CO increases on average ~60% during the morning rush hour, the concentration of black carbon may be about 60% higher than during the night. During the night of 19 June, the production rate of HONO was ~0.5 ppbv/hr or 3.4×10^6 molecules cm^{-3} s^{-1}. Ammann *et al.* (1998) found the production rate of HONO was first order in NO_2 and on the surface area of the fresh black carbon particles. Since the production of black carbon near York University is primarily due to diesel combustion, and the size distribution is likely constant, it follows that the rate of HONO production would be first order in the number of soot particles. Therefore, the HONO production rate would increase to $\sim 1.6 \times 10^7$ molecules cm^{-3} s^{-1} during the morning rush hour. This is lower than the production rate of $\sim 2.8 \times 10^7$ molecules cm^{-3} s^{-1} which would be required to maintain 1 ppbv of HONO at 8 a.m. However, with a 50% attenuation of the solar radiation by NO_2, the values are in good agreement.

3.3. ROLE OF HONO PHOTOLYSIS IN OH PRODUCTION

The role that HONO plays in OH production can be estimated by comparing the OH production from 1 ppbv HONO with that from 5 ppbv HCHO and 40 ppbv O_3 starting at 6 a.m. without solar attenuation and including a 0.5 ppbv/hr production rate for HONO (Figure 8). The production rate of OH from HONO maximizes at about 8×10^6 molecules cm^{-3} s^{-1} near 6:30 a.m. before rapidly decreasing to about 3.5×10^6 molecules cm^{-3} s^{-1} near 7:00 a.m. Near 8:30 a.m., ozone photolysis becomes the dominant OH production source. If we compare this to the OH produced by the photolysis of the measured HONO during the morning of 19 June, we see that the increased production rate of HONO results in an increase in the production rate of OH, however, ozone still becomes the dominant source of OH by around 9 a.m.

As an estimate of the role of HONO in the production of OH during mid day in the summer we can use the night-time production rate for HONO of 0.5 ppbv/hr or 3.4×10^6 molecules cm^{-3} s^{-1}, as an upper limit, since the NO_2 concentration is generally lower in the day than the night. For comparison, in summer, OH production rates by ozone photolysis result in production rates of $\sim 9 \times 10^7$ molecules cm^{-3} s^{-1} (Seinfeld and Pandis, 1998). Therefore in the summer, noontime OH

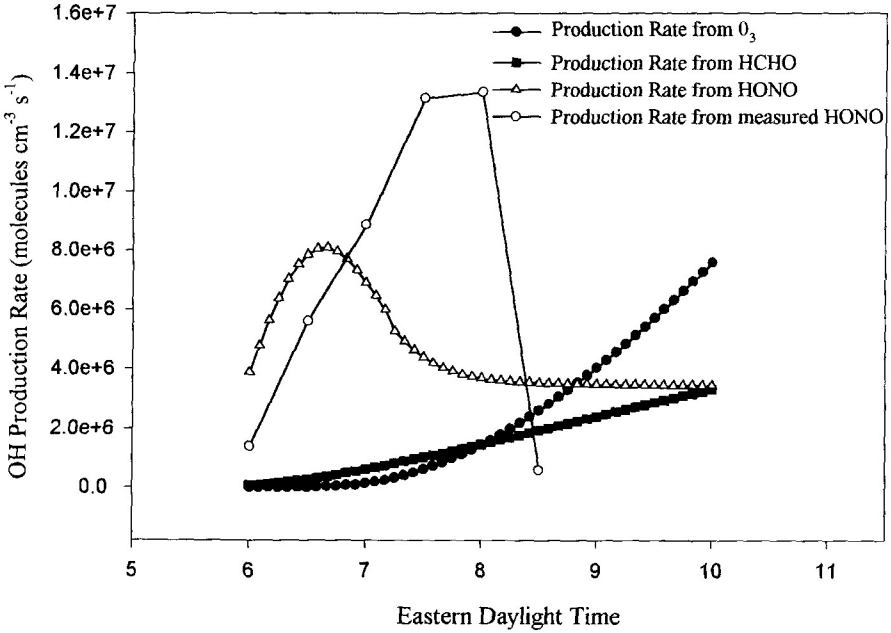

Figure 8. OH production rate from the photolysis of 40 ppbv of ozone (filled circle), 1 ppbv of HCHO (filled square), and 1 ppbv of HONO (unfilled triangle), and the measured HONO (unfilled circle) on the morning of 19 June 1998 after taking into account a 50% attenuation in solar radiation.

production by HONO is only ~5% of that by ozone photolysis, however it may be significant during low photolysis periods, such as mornings, evenings, cloudy conditions, and in the winter.

If the production of HONO in cities is dominated by the reaction of NO_2 on black carbon, then production should be relatively constant throughout the year. Since HONO photolyzes in the visible, unlike ozone and formaldehyde, there should be considerable HONO photolysis and therefore OH production in the winter. If the OH production rate of 3.4×10^6 molecules cm^{-3} s^{-1} from HONO occurred in winter, then the production of OH from HONO would be the dominant source of OH in cities during the winter. In the winter, at high latitudes, a large portion of rush hour would occur before sunrise, which may lead to very large concentrations of HONO in the early morning. Febo *et al.* (1996), measured night time HONO mixing ratios of near 10 ppbv in Milan, Italy in March, with daytime concentrations as high as 4 ppbv. On clear winter days in Toronto, the photolysis rate of HONO peaks at about 1.3×10^{-3} s^{-1}, resulting in a lifetime of ~13 minutes, which leads to noon concentrations of ~100 ppt of HONO. With the increased sensitivity of our instrument due to recent upgrading, winter daytime measurements of HONO should be possible.

4. Conclusions

Atmospheric HONO has been successfully measured at sub-ppbv levels using tunable diode laser spectroscopy. The ν_3 band, centred near 1263 cm^{-1}, has several lines in the R-branch near 1280 cm^{-1} which are sufficiently strong and interference free to measure HONO at ambient concentrations. Utilizing one of these lines, ambient HONO was measured with 30 minute time resolution at mixing ratios from the detection limit of 300 pptv to 1.9 ppbv.

HONO night-time production was measured at a rate of 0.5 ppbv/hr. This rate appeared to increase to near 2 ppbv/hr during the morning rush hour. The usual decrease in HONO after sunrise was delayed by a few hours, possibly due to a combination of an increase in the production rate of HONO with rush hour, and attenuation of the early morning light by high NO_2 within the aerosol haze/fog. Conditions favourable for HONO buildup, high NO_2 and aerosol, may also attenuate the incoming solar radiation, resulting in the longest delays of HONO photolysis after sunrise.

Acknowledgements

This research was funded in part by the National Science and Engineering Research Council (NSERC). We greatly appreciated the use of a diode laser made available by Dr D. R. Hastie, and for continued use of the Tunable Diode Laser Spectrometer and the mobile lab on loan from Dr Kurt Anlauf, Atmospheric Environment Services of Environment Canada. We also appreciated the uses of the NAPS 1998 data made available by John Shelton, Environment Canada. I would like to thank Dr Erik Griffioen and Dr J. McConnell for model runs to assess the impact of aerosols on the attenuation of solar radiation and Apollo Tang for calculation of the J values. Thanks to the Department of Chemistry at York University for the use of the IC, and Lucie Masciello for help with the IC analysis.

References

Akimoto, H., Takagi, H., and Sakamaki, F., 1987: Photo enhancement of the nitrous acid formation in the surface reaction of nitrogen dioxide and water vapour: Extra radical source in smog chamber experiments, *Int. J. Chem. Kinet.* **19**, 539–551.

Allegrini, I., Desantis, F., Dipalo, V., Febo, A., Liberti, A., Perrino, C., and Possanzini, M., 1987: Annular denuder method for sampling reactive gases and aerosols in the atmosphere, *Sci. Total Environ.* **67**, 1–16.

Ammann, M., Kalberer, M., Jost, D. T., Tobler, L., Rössler, E., Piguet, D., Gäggeler, H. W., and Baltensperger, U., 1998: Heterogeneous production of nitrous acid on soot in polluted air masses, *Nature* **395**, 157–160.

Andrés-Hernández, M. D., Notholt, J., Hjorth, J., and Schrems, O., 1996: A DOAS study on the origin of nitrous acid at urban and non-urban sites, *Atmos. Environ.* **30**, 175–180.

Appel, B. R., Winer, A. M., Tokiwa, Y., and Biermann, H. W., 1990: Comparison of atmospheric nitrous acid measurements by annular denuder and differential optical absorption systems, *Atmos. Environ.* **24A**, 611–616.

Barney, W. S., Wingen, L. M., Lakin, M. J., Brauers, T., Stutz, J., and Finlayson-Pitts, B. J., 2000: Infrared absorption cross-section measurements for nitrous acid (HONO) at room temperature, *J. Phys. Chem. A.* **104**, 1692.

Becker, K. H., Kleffmann, J., Kurtenbach, R., Weisen, P., Febo, A., Gherardi, M., and Sparapani, R., 1995: Line strength measurements of trans-HONO near 1255 cm^{-1} by tunable diode laser spectrometry, *Geophys. Res. Lett.* **22**, 2485–2488.

Berner, A., Sidla, S., Galambos, Z., Kruisz, C., Hitzenberger, R., Tenbrink, H. M., and Kos, G. P. A., 1996: Modal character of atmospheric black carbon size distributions, *J. Geophys. Res.* **101**, 19559–19565.

Brassington, D. J., 1994: Tunable diode laser absorption spectroscopy for the measurement of atmospheric species, *Adv. Spectrosc.* **24**, 1.

Chan, W. H., Nordstrom, R. J., Calvert, J. G., and Shaw, J. H., 1976: Kinetic study of HONO formation and decay reactions in gaseous mixtures of HONO, NO, NO_2, H_2O and N_2, *Environ. Sci. Technol.* **10**, 674–682.

Collett, J. L. Jr., Bator, A., Rao, X., and Demoz, B., 1994: Acidity variations across the cloud drop size spectrum, and their influence on rates of atmospheric sulfate production, *Geophys. Res. Lett.* **21**, 2393–2396.

Febo, A., Perrino, C., and Allegrini, I., 1996: Measurements of nitrous acid in Milan, Italy, by DOAS and diffusion denuders, *Atmos. Environ.* **30**, 3599–3609.

Fried, A., McKeen, S., Sewell, S., Harder, J., Henry, B., Goldan, P., Kuster, W., Williams, E., Baumann, K., Shetter, R., and Cantrell, C., 1997: Photochemistry of formaldehyde during the 1993 Tropospheric OH Photochemistry Experiment, *J. Geophys. Res.* **102**, 6283–6296.

Harris, G. W., Carter, W. P. L., Winer, A. M., Pitts, J. N. Jr., Platt, U., and Perner, D., 1982: Observations of nitrous acid in the Los Angeles atmosphere and the implications for the ozone precursor relationships, *Environ. Sci. Technol.* **16**, 414–419.

Harris, G. W., Mackay, G. I., Iguchi, I., Mayne, L. K., and Schiff, H. I., 1989: Measurements of formaldehyde in the troposphere by tunable diode laser absorption spectroscopy, *J. Atmos. Chem.* **3**, 119–137.

Harris, G. W., Klemp, D., Zenker, T., Burrows, J. P., and Mathieu, B., 1992: Tunable diode laser measurements of trace gases during the 1988 Polarstern cruise and intercomparisons with other methods, *J. Atmos. Chem.* **15**, 315–326.

Harrison, R. M. and Kitto, A. N., 1994: Evidence for a surface source of atmospheric nitrous acid, *Atmos. Environ.* **28**, 1089–1094.

Henderson, G. S., Evans, W. F. J., McConnell, J. C., and Templeton, E. M. J., 1987: A numerical model for one dimensional simulation of stratospheric chemistry, *Atmos. Oceans* **25**, 427–459.

Jenkin, M. E., Cox, R. A., and Williams, D. J., 1988: Laboratory studies of the kinetics of formation of nitrous acid from the thermal reaction of nitrogen dioxide and water vapour, *Atmos. Environ.* **22**, 487–498.

Kagann, R. H. and Maki, A. G. J., 1983: Infrared absorption intensities of nitrous acid (HONO) fundamental bands, *Quant. Spectrosc. Radiat. Transfer* **30**, 37.

Kalberer, M., Annann, M., Arens, F., Gaggeler, H. W., and Baltensperger, U., 1999: Heterogeneous formation of nitrous acid (HONO) on soot aerosol particles, *J. Geophys. Res.* **104**, 13825–13832.

Kitto, A.-M. N. and Harrison, R. M., 1992: Nitrous and nitric acid measurements at sites in south-east England, *Atmos. Environ.* **26A**, 235–241.

Koutrakis, P., Brauer, M., Slater, J. L., Stone, C. L., Stevens, R. K. Wolfson, J. M., and Spengler, J. D., 1988: Evaluation of an annular denuder filter pack system to collect acidic aerosols and gases, *Environ. Sci. Technol.* **22**, 1463–1468.

Lammel, G. and Cape, J. N., 1996: A study on the origin of nitrous acid at urban and non-urban sites, *Chem. Soc. Rev.* **25**, 361.

Mackay, G. I., Karecki, D. R., and Schiff, H. I., 1996: Tunable diode laser absorption measurements of H_2O_2 and HCHO during the Mauna Loa Observatory Photochemistry Experiment, *J. Geophys. Res.* **101**, 14,721–14,728.

Maki, A. G., 1988: High Resolution measurements of the ν_2 band of HNO_3 and the ν_3 band of trans-HONO, *J. Mol. Spectrosc.* **127**, 104–111.

National Air Surveillance (NAPS) Sites 1998 data, John Shelton, Environment Canada, Analysis and Air Quality Division, private communication.

Perner, D. and Platt, U., 1979: Detection of nitrous acid in the atmosphere by differential optical absorption, *Geophys. Res. Lett.* **6**, 917–920.

Pitts, J., Sanhueza, E., Atkinson, R., Carter, W. P. L., Winer, A. M., Harris, G. W., and Plum, M. N., 1984: An investigation of the dark formation of nitrous acid in environmental chambers, *Int. J. Chem. Kinet.* **16**, 919–939.

Platt, U., 1996: The origin of nitrous and nitric acid in the atmosphere, in W. Jaeschke (ed.), *Chemistry of Multi Phase Atmosphere Systems*, Springer, Berlin, NATO-ASI series.

Platt, U., Perner, D., Harris, G., Winer, A. M., and Pitts, J. N. Jr., 1980: Observations of nitrous acid in urban atmospheres by differential optical absorption, *Nature* **285**, 312–314.

Rothman, L. S., Rinsland, C. P., Goldman, A., Massie, S. T., Edwards, D. P., Flaud, J.-M., Perrin, A., Camy-Peyret, C., Dana, V., Mandin, J.-Y.n, Schroeder, J., McCann, A., Gamache, R. R., Wattson, R. B., Yoshino, K., Chance, K. V., Jucks, K. W., Brown, L. R., Nemtchinov, V., and Varanasi, P., 1998: The HITRAN molecular spectroscopic database and HAWKS (HITRAN Atmospheric Workstation): 1996 Edition, *J. Quant. Spectro. Rad. Trans.* **60**, 665.

Saliba, N. A., Mochida, M., and Finlayson-Pitts, B. J., 2000: Laboratory studies of sources of NONO in polluted urban atmospheres, *Geophys. Res. Lett.* **27**, 3229–3232.

Sakamaki, F., Hatakeyama, S., and Akimoto, H., 1983: Formation of nitrous acid and nitric oxide in the heterogeneous dark reaction of nitrogen dioxide and water vapour in a smog chamber, *Int. J. Chem. Kinet.* **15**, 1013–1029.

Schiff, H. I., Hastie, D. R., Mackay, G. I., Iguchi, T., and Ridley, B. A., 1983: Tunable diode laser systems for measuring trace gases in tropospheric air, *Environ. Sci. Technol.* **17**, 352–364.

Schiff, H. I., 1992: Ground based measurements of atmospheric gases by spectroscopic methods, in *Berichte den Bunsen Gesellschaft fur Physikalishe Cheme – an International J. Phys. Chem.* **96**, 296–306.

Seinfeld, J. H. and Pandis, S. N., 1998: *Atmospheric Chemistry and Physics: From Air Pollution to Climate Change*, Wiley-Interscience, Toronto.

Sickles, J. E. and Hodson, L. L., 1989: Fate of nitrous acid on selected collection surfaces, *Atmos. Environ.* **23**, 2321–2324.

Slemr, F., Harris, G. W., Hastie, D. R., Mackay, G. I., and Schiff, H. I., 1986: Measurements of gas phase hydrogen peroxide in air by tunable diode laser spectroscopy, *J. Geophys. Res.* **91**, 5371–5378.

Sjödin, A. and Ferm, M., 1985: Measurement of nitrous acid in urban air, *Atmos. Environ.* **19**, 985–992.

Sjödin, A., 1988: Studies of the diurnal variation of nitrous acid in urban air, *Environ. Sci. Technol.* **22**, 1086–1089.

Stockwell, W. R. and Calvert, J. G., 1978: The near ultraviolet absorption spectrum of gaseous HONO and N_2O_3, *J. Photochem.*, 193.

Vecera, D. and Dasgupta, P. K., 1991: Measurement of ambient nitrous acid and a reliable calibration source for gaseous nitrous acid, *Environ. Sci. Technol.* **25**, 255–260.

Wingen, L. M., Barney, W. S., Lakin, M. J., Brauers, T., and Finlayson-Pitts, B. J., 2000: A unique method for Laboratory quantification of gaseous nitrous acid using the reaction $HONO + HCl \rightarrow ClNO + H_2O$, *J. Phys. Chem. A* **104**, 329.